A convolution method of calculating dose for 15-MV x rays

T. R. Mackie,[a] J. W. Scrimger, and J. J. Battista
Department of Medical Physics, Cross Cancer Institute, Edmonton, Alberta, Canada T6G 1Z2

Arrays were generated using the Monte Carlo method representing the energy absorbed throughout waterlike phantoms from charged particles and scatter radiation set in motion by primary interactions at one location. The resulting "dose spread arrays" were normalized to the collision fraction of the kinetic energy released by the primary photons. These arrays are convolved with the relative primary fluence interacting in a phantom to obtain three-dimensional dose distributions. The method gives good agreement for the 15-MV x-ray dose in electronic disequilibrium situations, such as the buildup region, near beam boundaries, and near low-density heterogeneities.

I. INTRODUCTION

Present dose calculation methods are based on the assumption that all of the charged-particle energy liberated by photon radiation is deposited locally at the site of interaction. While this assumption is acceptable for cobalt-60 radiation, it weakens for higher energy x-rays for which the range of charged particles set in motion can be several centimeters. The need for considering this nonlocal energy deposition has been documented.[1-4] Some photon dose calculation methods have accounted for electronic "buildup" longitudinally along the central axis, but none have rigorously treated the lateral spread of charged particles set in motion.[5,6] Young and Kornelson[7] have taken into account the dose reduction caused by a lack of charged particles equilibrium using a semiempirical "loss factor."

For photon energies comparable to those of cobalt-60 radiation, existing methods rely on measured tissue–air ratio (TAR) data that assume that the primary dose is equal to the TAR extrapolated to a "zero-area field." This leads to a number of technical and fundamental problems for higher energy photon beams. Firstly, the TAR concept is usually replaced by a tissue–phantom ratio (TPR) which is based on measurements made in a phantom. It becomes more difficult to separate the contributions of primary and scattered radiation because the increase in TPR caused by scatter within the phantom must be isolated from increases caused by external factors[8] (e.g., collimators). Furthermore, extrapolation to a zero-area field to obtain the primary dose is not physically acceptable because lateral electronic equilibrium is lost and the dose is greatly reduced.

In this work, a physically sound and consistent method has been developed which allows calculation of three-dimensional dose distributions in homogeneous or heterogeneous phantoms irradiated with rectangular or irregularly shaped fields of high-energy photons. The use of measured data as a data base is abandoned and replaced with data generated from first principles by Monte Carlo techniques. The Monte Carlo method is used to map the spatial distribution of charged-particle energy away from a primary photon interaction site. This distribution, called a primary dose spread array, is convolved spatially, with the kinetic energy released at all the primary interaction sites to yield the primary dose distribution. In a heterogeneous phantom, the dose spread arrays need to be modified during convolution.

Any current method separating primary from scatter dose can be improved with the methodology proposed here. Since convolution is a well understood and documented technique, there are conceptual advantages for implementing a convolution framework for the spread of energy due to scattered photons, as well as charged particles set in motion. (Dean has used this approach to find where the scatter dose was being absorbed from cobalt-60 primary photons interacting in one location of a water phantom.[9])

The proposed method was based on concepts which will not become obsolete as improved computational power becomes available. The fundamental reason for this is the sound physical basis of the Monte Carlo and convolution procedures. Another reason is an inherent flexibility to compromise between speed and accuracy. Therefore, as computers become faster, greater accuracy can be achieved without modifying the algorithm substantially.

II. PRIMARY DOSE SPREAD ARRAYS

A primary dose spread array (analogous to the point spread array used in image processing) is the three-dimensional spatial distribution of energy deposited by electrons and positrons which spread from the site of the primary photon interactions. It is generated by tracking the motion of charged particles away from primary interaction sites occurring within a cubic volume element (voxel). These charged particles are followed, using the Monte Carlo method, in a homogeneous phantom consisting of voxels of the same size, atomic number, and density. The amount of energy deposited at, and in the neighborhood of, the interaction voxel is scored. Figure 1 illustrates the procedure schematically.

The incident photon fluence spectrum was not known and could not easily be measured. However, the spectrum was chosen by comparing measured depth dose values with the results of "electron gamma shower" (EGS) Monte Carlo sim-
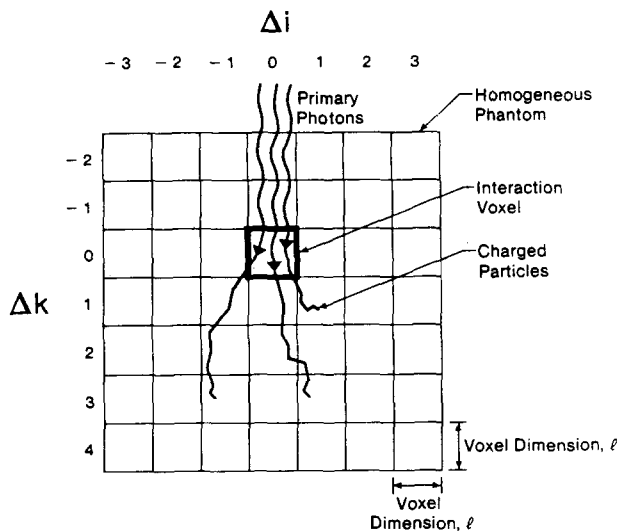
FIG. 1. Schematic representation of the generation of a primary dose spread array.
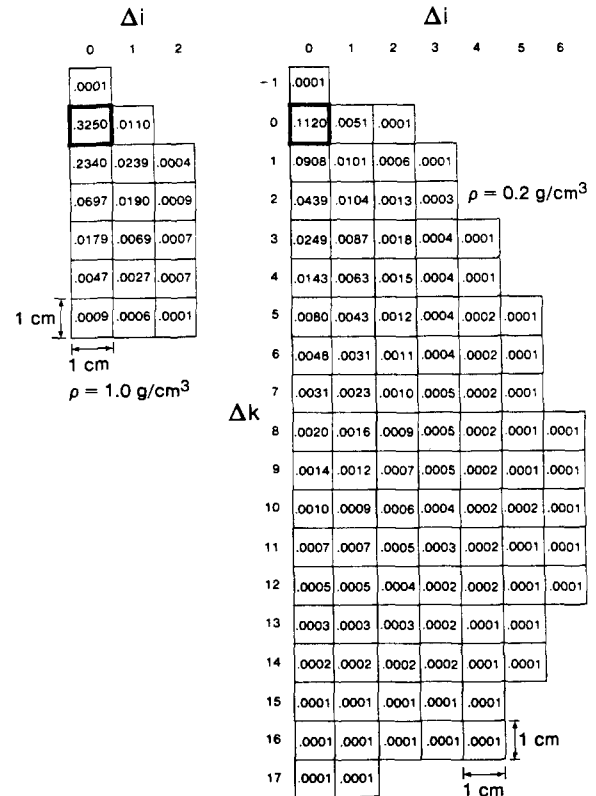
FIG. 2. Primary dose spread arrays. The numbers represent the dose deposited in the voxel normalized to the collision KERMA in the interaction voxel (bold borders).

ulations with various monoenergetic photon energies. (The 15-MV photon beam was obtained from a Siemens Mevatron-77. The measuring device was a Capintec PR-06C ion chamber with a Capintec 192A electrometer.) The EGS code was developed originally at Stanford University by Ford and Nelson,[10] and modified by Rogers at the National Research Council of Canada.[11,12] A monoenergetic 5.0-MeV beam duplicates the measured depth dose for a 15-MV x-ray beam to within 5% at depths up to 20 cm for a field size of 10 × 10 cm. (The EGS program employed cylindrical geometry so the equivalent circular field was used to model rectangular fields.[13]) A mixture of monoenergetic incident photon energies of 0.18, 0.67, 2.57, 6.61, 11.12, and 13.78 MeV with the photon fluence weighted in the proportions 0:11:11:11:5:0, respectively, improved the agreement to within 0.5%.

The dose spread arrays were actually generated by a homemade Monte Carlo code called MOCA, developed in our Institute. Both MOCA and EGS take into account the photoelectric effect, Compton effect, and pair production. EGS distinguishes positrons from electrons, whereas MOCA transports positrons as if they were electrons. Both programs produce photons when the positron annihilates. MOCA employs the approximations of continuous slowing down (without generation of secondary "knock-on" electrons) and Gaussian lateral scattering for charged particles. Bremsstrahlung was not included in MOCA.

Figure 2 shows voxel elements of two primary dose spread arrays for a pencil beam of 15-MV x rays interacting in a homogeneous phantom with cubic voxel dimensions of 1.0 cm. The density of the array on the left is 1.0 g/cm³, and that on the right is 0.2 g/cm³. The two media are assumed to be waterlike in chemical composition. The voxels shown in Fig. 2 are in the same plane as the interaction voxel. The beams have the same cross-sectional area as the voxels, and are made to interact only in the interaction voxel (bold borders). At least 10⁶ charged particles/cm² were set in motion by primary photons to generate these arrays. The dose spread arrays are quadrilaterally symmetric about the primary photon direction, which is designated as the Δk axis. To speed up

the convolution process for rectangular fields, the dose spread arrays are produced in a three-dimensional Cartesian geometry.

Figure 2 clearly illustrates that the assumption of local energy deposition at 15 MV is untenable. The value of the dose spread array at the interaction voxel (location 0, 0, 0) in a 1.0 g/cm³ phantom with a voxel size of 1 cm is 0.325, which indicates that 32.5% of the energy released at the interaction site is deposited there. The value at the same location for a 0.2 g/cm³ phantom with a voxel size of 1 cm is only 0.112. The maximum longitudinal range of charged particles set in motion in a 1.0 g/cm³ phantom is about 4–6 cm, and in a 0.2 g/cm³ phantom, the maximum longitudinal range is about 16–18 cm! In the lateral direction, charged particles can contribute to dose about 1–3 cm and 5–7 cm from the interaction site for 1.0 g/cm³ and 0.2 g/cm³ phantoms, respectively.

The primary dose spread array values indicate the primary energy deposited in each voxel normalized to the total energy released in the interaction voxel

$$Ap(\rho, l, \Delta i, \Delta j, \Delta k) = \frac{T(\rho, l, \Delta i, \Delta j, \Delta k)}{KER_c(\rho, l, 0, 0, 0)},$$ (1)

where $Ap(\rho, l, \Delta i, \Delta j, \Delta k)$ is the primary dose spread array at a distance $\Delta i, \Delta j, \Delta k$ from the interaction voxel, $T(\rho, l, \Delta i, \Delta j, \Delta k)$ is the energy deposited at the site, and $KER_c(\rho, l, 0, 0, 0)$ is the total energy of charged particles set in motion at the interaction site that is lost to electron collisions (not bremsstrahlung) in the phantom.[14]

Since the phantom is homogeneous, the interaction and dose deposition voxels have the same density. Therefore, the

array value is also equal to the dose deposited due to electron collisions in the neighboring voxels per unit kinetic energy released per unit mass, K_c (collision KERMA), at the interaction voxel.[14] If the dose spread arrays are spatially invariant (see Appendix) Eq. (1) can be expressed as

$$Ap\ (\rho, l, \Delta i, \Delta j, \Delta k) =$$
$$\frac{\text{DOSE}\ (\rho, l, i + \Delta i, j + \Delta j, k + \Delta k)}{K_c\ (\rho, l, i, j, k)}. \tag{2}$$

The primary dose spread arrays can be produced for different voxel dimensions and for a variety of waterlike phantoms with different densities. Figure 3 illustrates the dose spread arrays with a voxel and beam dimension of 5.0 cm and a density of 0.2 g/cm³. The values of the dose spread array elements of Fig. 3 are nearly equal to those of Fig. 2 (left). Therefore the product of the phantom density, ρ (g/cm³), and the voxel dimension, l (cm), is a fundamental measure of the voxel "size" in units of g/cm². O'Connor proposed that for photon beams, the dose in two media with different densities (but with the same atomic number) will be the same provided all dimensions in the media are scaled inversely with the density of the media.[15] The basis for the theorem was the linear dependence of the attenuation coefficient on density. O'Connor's theorem can now be said to be independent of the state of electronic equilibrium. This is expected because for a material of fixed atomic number, both the stopping power and the angular scattering power are directly proportional to the physical density.[16] This has also been shown experimentally by Young and Kornelson.[3,7]

The primary dose spread arrays are stored for various values of voxel size expressed in units of $\rho{\cdot}l$ (from $\rho{\cdot}l = 0.2$ to 1.0 g/cm² in step sizes of 0.2 g/cm²). This allows flexibility in the choice of voxel dimensions for dose computations and hence the spacing of calculation points. For example, a choice of a voxel size of 0.2 g/cm² can be used either for a medium with $\rho = 1.0$ g/cm³, to establish calculation points spaced at a distance of 0.2 cm, or in a medium with $\rho = 0.2$ g/cm³, for calculation points spaced 1 cm apart. When the desired spatial resolution and density yields a value of $\rho{\cdot}l$ which has not been stored, the dose spread array values need to be interpolated from the stored arrays.
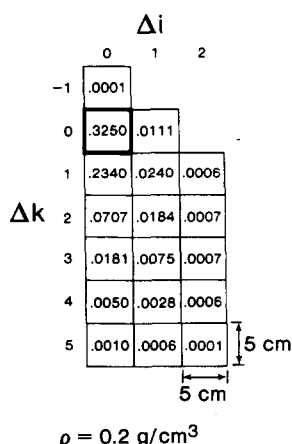
III. SCATTER DOSE SPREAD ARRAYS

The Monte Carlo program used to determine the primary dose spread arrays is also used to follow scattered photons and charged particles produced by the scatter photon interactions. The first scattered dose is scored separately from higher order multiple scatter. The dose due to first-scatter photons, which is deposited relatively close to the primary interaction site, is placed in a truncated first-scatter (TFS) dose spread array. The first-scatter dose deposited relatively far from the primary interaction site is included with multiple scatter in a residual first- and multiple-scatter (RFMS) dose spread array. Positron annihilation photons are treated as if they were multiply scattered photons. Since first-scattered photons are mainly forward directed, the location of the interaction voxel within the dose spread array has been optimized so that more voxels of the TFS dose spread array are scored "downstream" of the primary interaction site than "upstream."

The bulk of first-scatter photons has been separated from the multiple-scatter photons because of their different spatial distribution and magnitude of contribution to the total dose.[17] Separating most of the first scatter from multiple scatter also allows a choice of optimal sizes for each type of dose spread array; having a high spatial resolution when little dose is being deposited is not an effective use of computation time.[18] The size of the TFS dose spread array and the voxel dimension of both the scatter dose spread arrays and the primary dose spread arrays are selected to compromise speed and accuracy. The more elements in the TFS dose spread array, the slower the convolution calculation. The TFS dose spread array voxel dimension can be made smaller than in the RFMS dose spread array, reflecting its proximity and greater importance in contributing to the total dose. The TFS dose spread array is produced and stored for the same $\rho{\cdot}l$ values as the primary dose spread array, whereas the RFMS dose spread array is stored for values of $\rho{\cdot}l$ from 1.0 to 5.0 g/cm² in steps of 1.0 g/cm². The TFS dose spread array may be truncated without compromising too much accuracy because most first-scatter dose is deposited close to the primary interaction site.[17] The total lateral size of the RFMS dose spread array must be at least twice that of the largest field in which the dose is to be calculated.

Figures 4 and 5 illustrate examples of the TFS and RFMS dose spread arrays, respectively. The TFS dose spread array has a $\rho{\cdot}l$ value of 1.0 g/cm², and the RFMS dose spread array $\rho{\cdot}l$ value is 5.0 g/cm². They are displayed in an isodose format. The TFS dose spread array illustrated has a total width of 13 cm and a total height of 20 cm. Any first-scatter photon energy not deposited within its boundary is included with the RFMS dose spread array. The energy deposited by scattered photons has been normalized to the same quantity as the primary dose spread array, namely, to the collision fraction of the total charged particle energy released by primary photons.

Δi

	0	1	2
−1	.0001		
0	.3250	.0111	
1	.2340	.0240	.0006
2	.0707	.0184	.0007
3	.0181	.0075	.0007
4	.0050	.0028	.0006
5	.0010	.0006	.0001

Δk

5 cm

5 cm

$\rho = 0.2$ g/cm³

FIG. 3. This primary dose spread array equals the primary dose spread array in Fig. 2 (left) because they have the same $\rho{\cdot}l$ value.

IV. CONVOLUTION DOSE CALCULATION IN A HOMOGENEOUS PHANTOM

The dose spread arrays can be viewed as the response throughout all the voxels in the phantom to a primary pho-
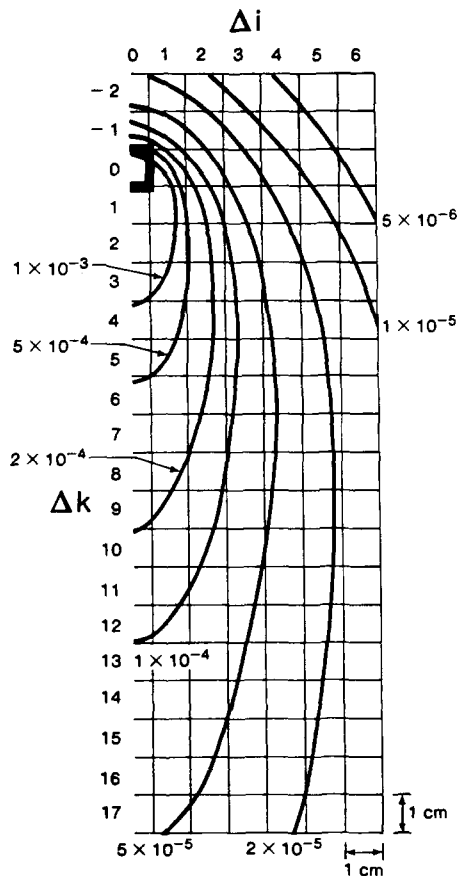
FIG. 4. Truncated first-scatter (TFS) dose spread array in isodose format.
$\rho = 1.0$ g/cm^3; $\rho \cdot l = 1.0$ g/cm^2.
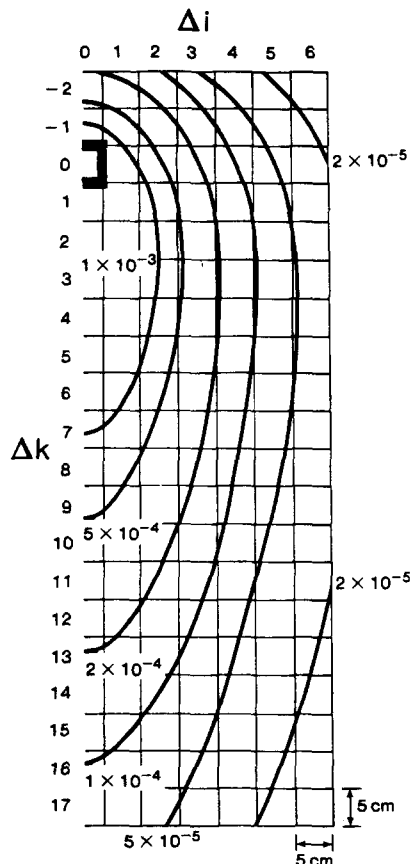

FIG. 5. Residual first- and multiple-scatter (RFMS) dose spread array in isodose format. $\rho = 1.0$ g/cm^3; $\rho \cdot l = 5.0$ g/cm^2.

ton "impulse" occurring in one voxel. The dose spread arrays can be used as the kernel in a convolution calculation to produce a three-dimensional dose distribution. The dose contribution to a dose deposition voxel, $i + \Delta i$, $j + \Delta j$, $k + \Delta k$, due to primary interactions at a voxel i, j, k in a homogeneous water phantom, is illustrated in Fig. 6 and given by

Dose contribution $(i + \Delta i, j + \Delta j, k + \Delta k)$

$$= K_c (\rho \cdot l = l, i, j, k) A (\rho \cdot l = l, \Delta i, \Delta j, \Delta k). \qquad (3)$$

The density ρ is now interpreted as the gravimetric density relative to water. Equation (3) can be used to generate the absolute dose. However, usually only the relative dose distribution is required. If beam "hardening" is negligible (see Appendix), $K_c (\rho \cdot l = l, i, j, k)$ may be replaced by the relative primary photon fluence

$$\Phi'(i, j, k) = \frac{\Phi(i, j k)}{\Phi(0,0,0)}. \qquad (4)$$

The relative fluence $\Phi'(i, j, k)$ is the primary photon fluence at the interaction voxel normalized to the incident primary fluence at the central axis. $\Phi'(i, j, k)$ takes into account the photon attenuation and inverse square reduction (for a divergent beam) of the primary fluence. It also accounts for the external contour of the patient and for beam modifying devices, such as shielding, which alters the relative fluence but does not alter the dose spread arrays. Including the dose spread array, Eq. (3) now becomes

Dose contribution $(i + \Delta i, j + \Delta j, k + \Delta k)$

$$\propto \Phi'(i, j, k) A (\rho \cdot l = l, \Delta i, \Delta j, \Delta k). \qquad (5)$$

The convolution of the dose spread arrays with the relative fluence can proceed in two different ways: the interaction point of view and the dose deposition point of view. In general, the calculation may be done by either method, but there are circumstances where one approach is more efficient.

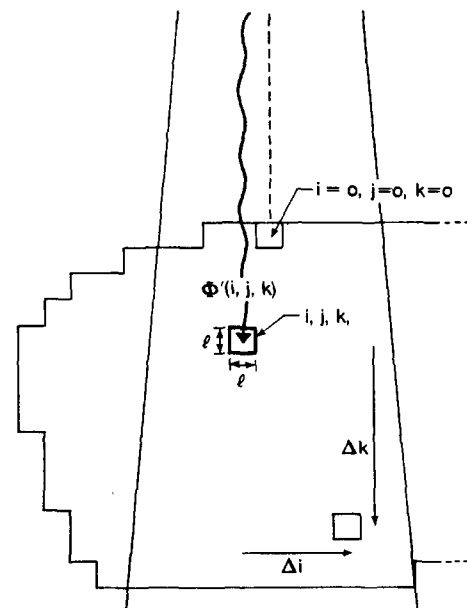In the interaction point of view, the macroscopic beam is

FIG. 6. Calculation using the interaction point of view.

composed of a set of contiguous pencil beams, each of which is followed through the phantom to see where the primary interactions occur. The dose spread array contributions throughout the phantom are summed for all such pencil beams. The dose in the interaction point of view is

$$\text{Dose } (i + \Delta i, j + \Delta j, k + \Delta k)$$

$$\propto \sum_i \sum_j \left[\sum_k \Phi'(i,j,k)A\ (\rho \cdot l = l,\Delta i,\Delta j,\Delta k) \right], \qquad (6)$$

where the i,j,k summation is over all interaction voxels, i.e., those voxels inside the phantom and the field boundary. Depending on the region of interest, the dose outside the beam boundary can also be computed.

Figure 6 illustrates the calculation of dose using the interaction point of view. The relative fluence is calculated for each point along a pencil beam [inside square brackets in Eq. (6)] by following the primary pencil beams through the phantom. When a beam blocking device, such as a compensator, is introduced in the beam, some of the primary pencil beams are affected. The interaction point of view can determine the effect of changed primary pencil beams on the dose throughout the phantom without recalculating the entire beam.

The interaction point of view gives the dose throughout a region of interest. Often, only the dose at a few voxels is desired. In this case, the dose in these voxels is calculated using the dose deposition point of view.

In a homogeneous, unbounded phantom there is a geometrical reciprocity between the primary interaction and dose deposition voxels. Even though the dose spread arrays were produced to describe the transport and absorption of dose throughout a phantom due to primary interactions at a voxel, they also describe the absorption of dose in a voxel due to an equal magnitude of primary interactions throughout the phantom. This is essentially the same principle as the source–target reciprocity used in health physics to calculate the organ dose to internal isotopes.[19] [The source–target reciprocity only rigorously applies to the RFMS dose spread array when the phantom is infinite (see Appendix)].

Figure 7 illustrates the use of the dose spread arrays from the dose deposition point of view. The dose spread arrays now represent the dose deposited in the dose deposition voxel normalized to the collision KERMA produced in the interaction voxels. The dose-deposition point-of-view calculation sums the dose contribution at the dose deposition voxel due to primary interactions throughout the phantom. The dose at a point I, J, K is given by

$$\text{Dose } (I, J, K)$$

$$\propto \sum_{\Delta i} \sum_{\Delta j} \sum_{\Delta k} \Phi'(I - \Delta i, J - \Delta j, K - \Delta k)$$

$$\times A\ (\rho \cdot l = l, \Delta i, \Delta j, \Delta k). \qquad (7)$$

If the dose at only a few voxels is required, the dose deposition point of view is more efficient. For example, the dose deposition point of view may be used when determining the dose along the central axis. The dose deposition point of view is mathematically equivalent to taking the convolution using the serial product.[20] A disadvantage to calculating the dose distribution throughout a large volume using the dose depo-
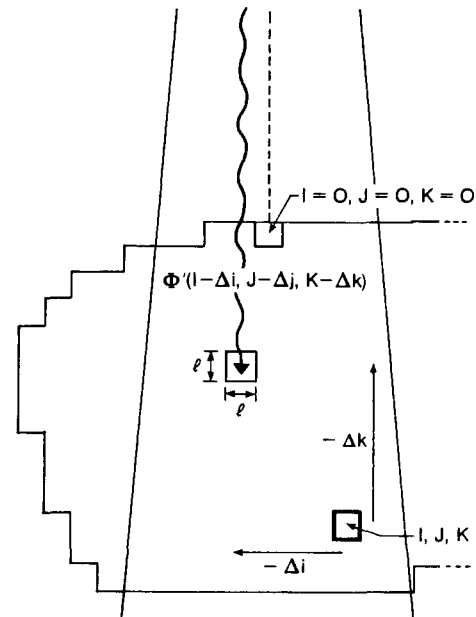
FIG. 7. Calculation using the dose deposition point of view.

sition point of view is that a large array for the relative fluence must be precalculated and stored before Eq. (7) can be used.

Eqs. (5), (6), and (7) do not specify which dose spread array is being convolved. The same general equations apply to all the dose spread arrays, except that the number of terms in the summation and the value of the relative fluence will depend on the voxel dimension of the dose spread array.

Figure 8 illustrates the measured and calculated tissue-maximum ratio (TMR) as a function of depth in a homogen-
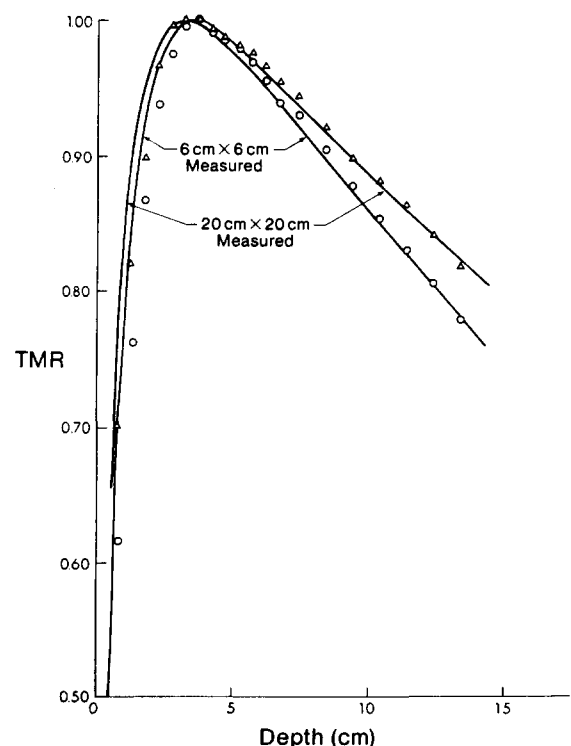

FIG. 8. Tissue-maximum ratio (TMR) at 15 MV as a function of depth. $O = 6 \times 6$ cm calculated; $\triangle = 20 \times 20$ cm calculated.

eous water phantom along the beam central axis for field sizes of 6×6 cm and 20×20 cm. The calculated TMR data were obtained by assuming that the beam was parallel (see Appendix) and had no inverse square reduction of the fluence with depth. The agreement between the measured and calculated dose is better than 1% beyond d_{max}, and within 10% in the buildup region.

The effective mass attenuation coefficient was calculated from the spectrum. Due to hardening (see Appendix), this quantity varies between 0.033 and 0.029 cm^2/g for depths of 0 and 30 cm, respectively. A constant value of 0.031 cm^2/g, calculated for a depth of 10 cm, was used. This is nearly the same value obtained for the same accelerator by Paul et al., by fitting an effective mass attenuation coefficient to zero-area TMR data.[21]

Figure 9 illustrates dose profiles at d_{max} for field sizes of 10×10 cm and 30×30 cm. The fluence profile at the phantom surface was assumed to be uniform inside the beam boundary and zero outside the beam boundary. This assumption appears to be adequate for the 10×10 cm field, but does not account for the "horns" in the larger field profile. The falloff in dose near the beam boundaries, due to lateral electronic disequilibrium (*not* geometrical penumbra), is accounted for.

The method can also take into account irregularly shaped fields. Figure 10 illustrates the effect on the dose profile at a depth of 5 cm when a shield is placed in the beam. The shield consisted of a bar of cerrobend extending completely across the field in a transverse direction to the profile. The shielded width of the field was 1.5 cm, and the bar had a thickness of 8.5 cm. The primary fluence transmission through the cerrobend was calculated to be 3.1%. Figure 10 also illustrates a calculation of the profile, assuming the primary dose is deposited locally. The measured profile agrees best with the calculation using nonlocal primary energy deposition. This illustrates that charged particles are streaming into the region under the shield.
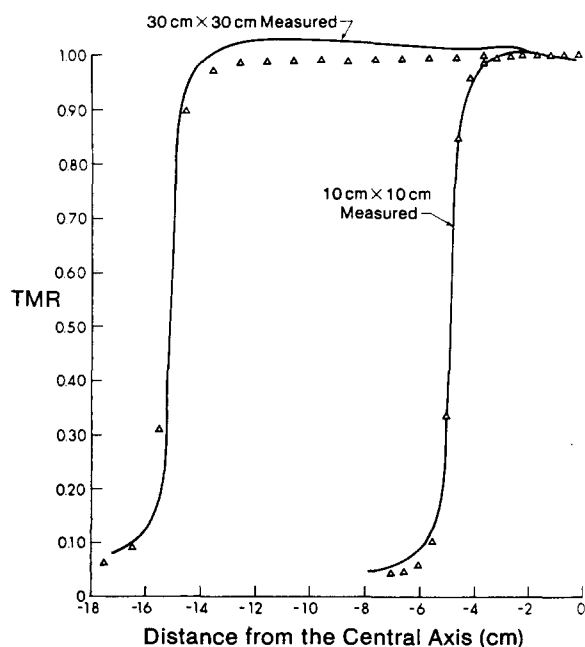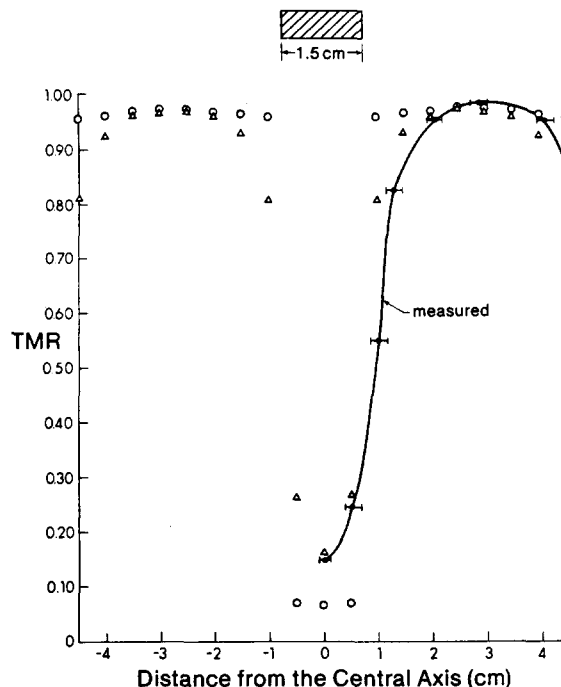

FIG. 10. 15-MV TMR profile at 5-cm depth when the central axis is shielded with 8.5 cm of cerrobend. The calculated value is done with local (O) and nonlocal (△) primary energy deposition.

V. EXTENSION TO HETEROGENEOUS MEDIA

Charged-particle transport through heterogeneous media is much more complex. To be rigorous, the primary dose spread arrays would have to be generated for each heterogenous situation that could be encountered. The number of possible combinations is enormous, so that an acceptable approximation is necessary to take advantage of data stored in the dose spread arrays, generated for homogeneous phantoms of different densities.

The extension of O'Connor's theorem for charged particles set in motion suggests that range scaling may be used to approximate charged-particle dose spread arrays in heterogeneous phantoms. The dose spread arrays stored for various values of $\rho \cdot l$ were, therefore, employed. The calculation resolution l is chosen and fixed at the start of the calculation. As shown in Fig. 11, the average density $\bar{\rho}$ between the interaction and dose deposition sites is found. The array value for the location, $\Delta i, \Delta j, \Delta k$, in a homogeneous phantom with the same $\bar{\rho} \cdot l$ value, is found by interpolating between dose spread arrays at fixed $\rho \cdot l$ values. Linear interpolation is satisfactory because the array values, as functions of $\rho \cdot l$, vary relatively slowly.

Interpolating to get a dose spread array valid for an average density between the interaction and dose deposition sites $\bar{\rho}$ implies that it has been normalized to the total amount of energy released in an interaction voxel of the same density. However, the density of the interaction voxel, $\rho(i, j, k)$, in a heterogeneous phantom is generally not the same as the average density between the interaction and dose deposition voxel. The primary dose contribution to a dose deposition voxel, due to primary interactions at an interaction voxel of density $\rho(i, j, k)$ when the average density between these voxels is $\bar{\rho}$, is given by

30 cm × 30 cm Measured

10 cm × 10 cm Measured

TMR

Distance from the Central Axis (cm)

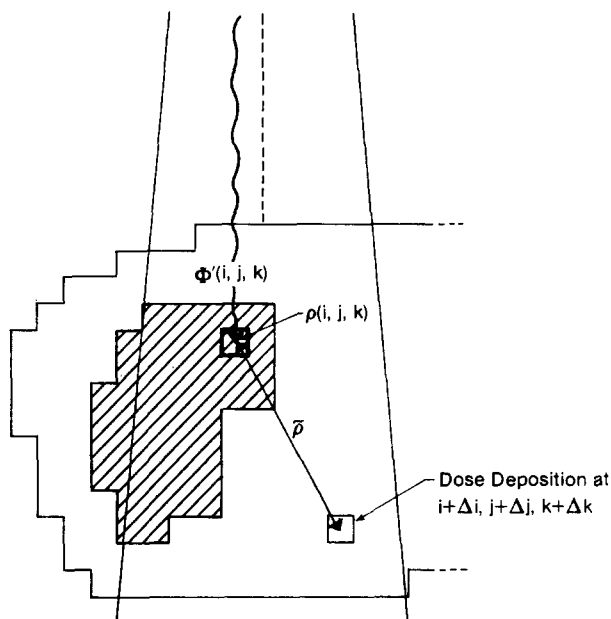FIG. 9. TMR profile at d_{max} for a 15-MV beam. △ = calculated.

FIG. 11. Illustration of the extension of the algorithm to waterlike heterogeneous media. $\bar{\rho}$ is the average density between the interaction and dose deposition voxels.
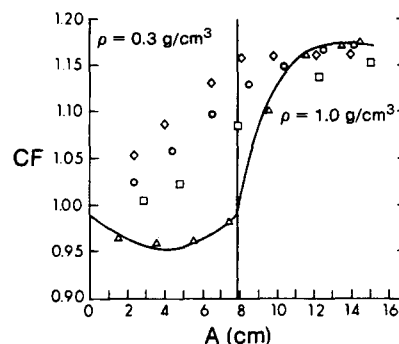

FIG. 12. Comparison of measured and various calculated correction factors (TMR in a heterogeneous medium normalized to the TMR in a unit-density medium) along the central axis. The measuring probe was kept at a constant 100 cm from the source. The thickness of overlying material was a constant 15.5 cm. The parameter A is the distance from the first interface to the probe. The field size is 5×5 cm. $\Diamond$ = TAR ratio; $\square$ = Batho; $\bigcirc$ = equivalent TAR; $\triangle$ = convolution; and —— = measured.

Dose contribution $(i + \Delta i, j + \Delta j, k + \Delta k)$

$$\propto \Phi'(i,j,k) \frac{\rho(i,j,k)}{\bar{\rho}} \Delta p(\bar{\rho}\cdot l, \Delta i, \Delta j, \Delta k). \tag{8}$$

(Note that the dose spread array value $\Delta p(\bar{\rho}\cdot l, \Delta i, \Delta j, \Delta k)$ is not invariant for the same value of $\Delta i, \Delta j, \Delta k$ at different values of i, j, k because $\bar{\rho}$ changes throughout the phantom. Convolution with a noninvariant kernel is called superposition.) The factor $\rho(i,j,k)/\bar{\rho}$ takes into account the difference in the amount of kinetic energy released in the heterogeneous interaction voxel compared to the amount set in motion in the interpolated homogeneous voxel of density $\bar{\rho}$. Otherwise, the calculation is carried out in the same manner as in a homogeneous phantom. Therefore, this procedure avoids the need to first compute the dose in water and then calculate a correction for inhomogeneity, separately.

The TFS dose spread array is scaled using the same algorithm. In fact, using this algorithm, the TFS dose spread array gives the exact correction. This is because a first-scatter photon interacting at the dose deposition voxel could not have interacted anywhere other than along the path between the primary interaction and dose deposition voxels. Since the same algorithm is used for the primary and TFS dose spread arrays, and they are stored for the same values of $\rho\cdot l$, these arrays may be combined where they coincide spatially. The TFS dose spread array need only be dealt with separately where it extends beyond the border of the primary dose spread array.

Multiple-scatter photons may have interacted anywhere within the phantom, not just between the primary interaction and dose deposition voxels.[22] Therefore, the average density of the *phantom* is used in Eq. (8) instead of the mean density along the path between the interaction and dose deposition voxels. This approximation is further justified because multiple scattering is a minority contribution to the total dose.[17] This approximation avoids calculating the

mean density between the interaction and dose deposition voxels of the RFMS dose spread array, resulting in a saving of computation time.

Figures 12 and 13 illustrate the TMR correction factor along the central axis for a heterogeneous phantom consisting of horizontal slabs of low- and unit-density materials for field sizes of 5×5 and 10×10 cm. The experimental measurements were obtained using cork and polystyrene slabs. No buildup cap was used on the ion chamber when measuring the dose in cork. The cork density was measured gravimetrically to be 0.30 ± 0.02 g/cm³. The ion chamber was kept at a constant distance of 100 cm from the source, and the position of the cork region, with respect to the chamber, was varied. The parameter A is the distance from the first cork interface to the ion chamber. The cork thickness was 7.90 ± 0.2 cm. The correction factor (CF) is the dose in the heterogeneous phantom normalized to the dose in a unit-density homogeneous phantom. The correction factor is less than 1.0 in cork at 5×5 cm, which indicates that the dose to cork is less than the dose in the homogeneous phantom, even though the primary photon fluence is greater. This is due to a loss of lateral electronic equilibrium, because the distance from the central axis to the field boundary is smaller than the lateral range of charged particles. The doses calculated by some existing methods are shown for comparison in Figs. 12 and 13. The existing methods assume electronic equilibrium, and poorly predict the dose in this situation. The convolu-
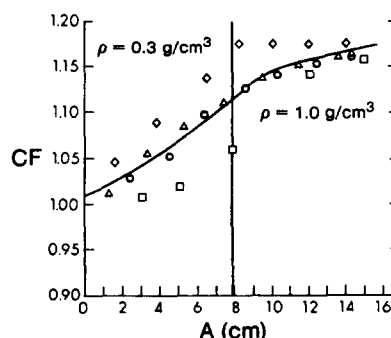

FIG. 13. Same as Fig. 12, except the field size is 10×10 cm.

tion calculation predicts not only the correct trend but also the measured correction factor to within 2%. Lateral equilibrium is established at a field of 10×10 cm, and for this situation, the convolution calculation and the equivalent TAR methods both predict the dose adequately.

VI. DISCUSSION

The dose spread arrays are "synthetic" macroscopic data, determined from the microscopic transport of individual particles, using the Monte Carlo method. This information cannot be obtained from measurement because a real primary photon beam cannot be forced to interact at only one region of the material. This requirement is necessary in order to describe the transport of secondary particles set in motion by primary photon interactions. All the dose spread arrays were generated with the inclusion of charged particle transport. The primary dose spread array is proportional to the energy deposited by charged particles set in motion by primary photons. The scatter dose spread arrays are proportional to the energy deposited by charged particles set in motion by scattered photons. An analytic solution to photon-charged-particle transport would be difficult (if not impossible) to obtain.[23] For this reason, the Monte Carlo method was used to generate all of the dose spread arrays.

The convolution procedure separates the photon-charged-particle transport into physically meaningful components. Primary photon interactions are separated from charged-particle and secondary photon transport and energy deposition.[23] This division of primary fluence from dose deposition is a more appropriate model of radiation transport than the modification of measured dose distributions, in which these two effects are combined. This does not undermine the importance of obtaining good measurements, since this provides the selection criteria for the photon spectrum used to compute the dose spread arrays.

The present method has been used to calculate the dose in waterlike heterogeneous media such as lung. The method could be extended to other media of different atomic composition, such as bone. The primary dose spread arrays may have to be recalculated for these types of tissues because charged-particle scattering is strongly dependent on atomic number. The scatter dose spread arrays would not likely be affected because the Compton scattering cross section per electron is approximately independent of atomic number.[24] The density ρ would now have to be interpreted as the electron density relative to water.[25] Two additional factors would have to be included in Eq. (8) when the primary dose is being calculated,

Dose contribution $(i + \Delta i,\ j + \Delta j,\ k + \Delta k)$

$$\propto \Phi'(i,j,k)\frac{\rho(i,j,k)}{\bar{\rho}}$$

$$\times \frac{[\bar{\mu}_{en}/\rho]_{Z(i,j,k)}}{[\bar{\mu}_{en}/\rho]_{\bar{Z}}} \times \frac{[\bar{S}/\rho]_{Z(i+\Delta i,j+\Delta j,k+\Delta k)}}{[\bar{S}/\rho]_{\bar{Z}}}$$

$$\times Ap(\bar{Z},\ \bar{\rho}\cdot l,\ \Delta i,\ \Delta j,\ \Delta k),$$

(9)

where $\bar{Z}$ is the average effective atomic number between the interaction and dose deposition sites. The first ratio takes into account the relative difference in the amount of energy released in the real interaction voxel of effective atomic number $Z(i,j,k)$, compared to the amount released in a homogeneous phantom of effective atomic number $\bar{Z}$. The second ratio takes into account the amount of energy deposited in the real dose deposition voxel of effective atomic number $Z(i + \Delta i, j + \Delta j, k + \Delta k)$, compared to the amount deposited in a homogeneous phantom of effective atomic number $\bar{Z}$.

Basing photon dose calculations on the firm mathematical foundation of convolution may allow additional future improvements. In *homogeneous* phantoms, the dose spread arrays are spatially invariant so that the relative fluence array and dose spread arrays may be Fourier transformed in the spatial frequency domain. The convolution may then proceed more quickly[26] by multiplying the transformed arrays. The dose can then be obtained by taking the inverse Fourier transform of the result. This procedure is used routinely in image processing applications.[20]

Deconvolution techniques may be useful in optimizing the delivery of radiation therapy. If one knows the attributes of an optimal dose distribution (e.g., uniform dose to the target volume and minimal dose to surrounding tissue), and the beam directions and intensities, the dose spread array can be deconvolved from the ideal dose distribution to obtain the best primary fluence distribution. This information could be used to design modifying devices, such as beam blocks, to approach the ideal relative fluence distribution in homogeneous or heterogeneous media.

ACKNOWLEDGMENTS

APPENDIX: THE SPATIAL INVARIANCE OF THE DOSE SPREAD ARRAYS

The dose spread arrays are produced using a very large phantom. The primary dose spread array is finite in extent so the phantom need only have been larger than the maximum range of charged particles set in motion. The TFS dose spread array is completely independent of the size of the phantom used in the simulation. The size of the phantom will affect the RFMS dose spread array only. The use of this dose spread array near the edge of the phantom will introduce error. However, since this dose spread array contributes a small fraction to the total dose, this error due to the extent of the phantom will be insignificant.

The dose spread arrays are not completely spatially invariant in homogeneous phantoms for two other reasons. Beam hardening is due to the preferential removal of low-energy photons interacting in the phantom. As the beam penetrates the phantom, it has a greater fraction of higher energy photons. Beam hardening effects were not included in the results described. If it is necessary to include hardening effects for
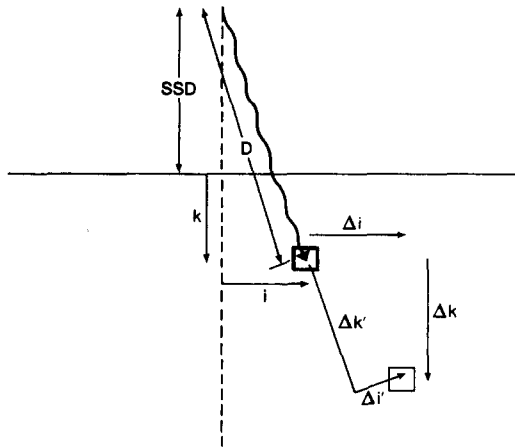
FIG. A1. Rotation of the dose spread arrays to take into account a divergent primary beam.

some beams, the convolution can proceed either using different dose spread arrays for different locations in the phantom or by repeating the calculation for each photon energy bin.

Divergent beams have three geometrical characteristics which distinguish them from parallel beams. There is an inverse square reduction of the primary photons and a linear increase in each field dimension as a function of depth. Another characteristic may have to be taken into account for this method. The dose spread arrays are not invariant for diverging beams. Figure A1 illustrates that a dose spread array should be tilted at an angle from the central axis to align it with the primary pencil beam. For example, the angle of tilt is about 8.5° at a distance of 100 cm from the source at the edge of a 30 × 30 cm field. To be rigorous, the dose spread array at $i + \Delta i, j + \Delta j, k + \Delta k$ should be transformed to $i + \Delta i', j + \Delta j', k + \Delta k'$, where

$$\Delta k' = \frac{(\text{SSD} + k)\Delta k + r \Delta r}{D}, \quad (\text{A1})$$

$$\Delta i' = \frac{\Delta i D - i \Delta k'}{\text{SSD} + k}, \quad (\text{A2})$$

$$\Delta j' = \frac{\Delta j D - j \Delta k'}{\text{SSD} + k}, \quad (\text{A3})$$

for $r = \sqrt{i^2 + j^2}$, $\Delta r = \sqrt{\Delta i^2 + \Delta j^2}$, and SSD is the source-to-surface distance. If $\Delta i'$, $\Delta j'$, or $\Delta k'$ is not an integer, interpo-

lation is necessary. This has not proven to be an important effect when calculating TMRs in the simple phantoms investigated so far. The transformation changes the value of the TMR at the central axis by less than 1%, up to a thickness of 20 cm in a 20 × 20 cm field at a distance of 100 cm from the source. However, this aspect of beam divergence may be an important effect when calculating percentage depth dose, or calculating dose in phantoms with complex heterogeneities.

[a] Presently at Department of Medical Physics, Allan Blair Memorial Clinic, Regina, Saskatchewan, Canada, S4T 7T1.
[1] J. Dutreix and M. Bernard, Br. J. Radiol. 39, 205 (1966).
[2] P. M. K. Leung, B. Seaman, and P. Robinson, Radiology 94, 449 (1970).
[3] R. O. Kornelsen and M. E. J. Young, Med. Phys. 9, 114 (1982).
[4] P. H. McGinley and M. Sanders, Med. Phys. 9, 738 (1982).
[5] F. Bagne, Med. Phys. 7, 664 (1980).
[6] T. R. Mackie and J. W. Scrimger, Med. Phys. 9, 620 (1982).
[7] M. E. J. Young and R. O. Kornelsen, Med. Phys. 10, 450 (1983).
[8] F. M. Khan, W. Sewchand, J. Lee, and J. F. Williamson, Med. Phys. 7, 230 (1980).
[9] R. D. Dean, Med. Phys. 7, 429 (1980).
[10] R. L. Ford and W. R. Nelson, The EGS Code System, Report No. 210, Stanford Linear Accelerator Center, Stanford, 1982.
[11] D. W. O. Rogers, Nucl. Instrum. Methods 199, 531 (1982).
[12] D. W. O. Rogers, A. F. Bielajew, and A. E. Nahum, in Proceedings of the Eighth International Conference in Radiation Therapy, Toronto, edited by J. R. Cunningham, D. Ragan, and J. Van Dyk (IEEE Computer Society, Toronto, 1984), p. 140.
[13] M. Cohen, D. E. A. Jones, and D. Greene, Br. J. Radiol. Suppl. 11, (1972).
[14] F. H. Attix, Health Phys. 36, 347 (1979).
[15] J. E. O'Connor, Phys. Med. Biol. 1, 352 (1957).
[16] International Commission on Radiation Units and Measurements Report No. 21, 1972, p.12.
[17] J. W. Wong, R. H. Henkelman, A. Fenster, and H. E. Johns, Med. Phys. 8, 775 (1981).
[18] P. Bloch and R. Wallace, Med. Phys. 6, 149 (1979).
[19] M. Cristy, Phys. Med. Biol. 28, 1289 (1983).
[20] R. Bracewell, The Fourier Transform and Its Applications (McGraw-Hill, New York, 1965).
[21] J. M. Paul, R. F. Koch, F. R. Khan, and B. S. Devi, Med. Phys. 10, 237 (1983).
[22] J. W. Wong, R. M. Henkelman, J. W. Andrew, J. Van Dyk, and H. E. Johns, Med. Phys. 8, 783 (1981).
[23] W. C. Roesch, Radiation Dosimetry, edited by F. H. Attix and W. C. Roesch (Academic, New York, 1968), p. 232.
[24] J. H. Hubbell, "Photon Cross Sections, Attenuation Coefficients, and Energy Absorption Coefficients From 10 keV to 100 GeV," Natl. Bur. Stand., (U.S.) Publ. No. NBS-29, 1969.
[25] M. R. Sontag and J. R. Cunningham, Med. Phys. 4, 431 (1977).
[26] A. L. Boyer and E. C. Mok, in Proceedings of the Eighth International Conference in Radiation Therapy, Toronto, edited by J. R. Cunningham, D. Ragan, and J. Van Dyk (IEEE Computer Society, Toronto, 1984), p. 14.